Original Article: An Amine/Imine Functionalized Microporous MOF as a New Fluorescent Probe Exhibiting Selective Sensing of Fe³⁺ and Al³⁺ Over Mixed Metal Ions

Vahid Safarifard * | **Yeganeh Davoudabadi Farahani**

Department of Chemistry, Iran University of Science and Technology, Tehran 16846-13114, Iran

A B S T R A C T

Nowadays metal-organic frameworks with multiple luminescent centers are very fascinating as multifunctional luminescent material because of their luminescence properties, which could be systematically tuned by deliberate use of organic ligands and metal ions. In this research, we explored a microporous mixed-ligand MOF for highly selective and sensitive detection of metal ions. A two-fold interpenetration pillared-layer amine/imine-functionalized MOF known as TMU-16-NH₂, $[Zn_2(NH_2\text{-}BDC)_2(4\text{-}bpdh)]\cdot 3DMF$, have been synthesized *via* a mixed ligand approach using amino-1,4-benzenedicarboxylate (NH₂-BDC) and 2,5-bis(4-pyridyl)-3,4-diaza-2,4-hexadiene (4-bpdh) under solvothermal condition. Sensor TMU-16-NH2 exhibits Al3+-selective TURN-ON and Fe³⁺-selective TURN-OFF type fluorescence emission responses, for which the electrostatic interaction between Fe³⁺ and Al³⁺ ions and the inner surface of the micropores may play a critical role. Moreover, the sensor TMU-16-NH₂ shows significantly color change from light yellow to orange and colorless with the addition of Fe³⁺ and Al³⁺ ions, respectively, which is distinguished by naked-eye. More significantly, the remarkable quenching and enhancing effects of TMU-16-NH₂ for Fe³⁺ and Al³⁺ possess the advantages of good selectivity, fast response time (<1min), low-cost, as well as very low detection limits of 0.7 and 0.09 µM for Fe³⁺ and Al³⁺, respectively. Interestingly, the probe exhibits high sensitivity for Fe³⁺ and Al³⁺ ions, which is far below WHO's acceptable limit in drinking water.

Introduction

Metal ions are required for the proper function of all cells within every living organism, and disruptions in localizations and concentrations of metal ion pools are a major contributor to aging and disease [1]. Transition metal ions like Fe³⁺ or Al³⁺ play a vital role in human life [2]. As known, iron, one of the most important and indispensable elements in metabolic processes, is extensively distributed in environmental and

Corresponding Author: Vahid Safarifard (vsafarifard@iust.ac.ir)

biological systems [3]. It plays significant part in oxygen metabolism, oxygen uptake, and electron transfer [4]. There approximately exists 4-5 g Fe in human body in different forms [5]. Iron deficiency and overload can both disturb the cellular homeostasis and induce various biological disorders [6]. A deficiency of iron limits oxygen delivery to cells, resulting in fatigue, poor work performance, and decreased immunity. Conversely, excess amounts of iron ions in a living cell can catalyze the production of reactive oxygen species (ROS) *via* the Fenton reaction, which can damage lipids, nucleic acids, and proteins [7-9]. On the other hand, aluminum is the third most abundant metal (after oxygen and silicon) in the earth's crust, accounting for approximately 8% of its mass [10]. The distribution of aluminum in the environment has been aggravated by the widespread use of aluminum-based materials in industrial applications, including paper, textiles, cosmetics and pharmaceuticals, and also for water treatment, in food additives and in the production of light alloys [11-12]. Nowadays, because of acidic rain and human activities in the environment, increasing exposure to free aluminum ions (Al^{3+}) poses a severe threat to biospheres and human health [13]. Excessive aluminum, especially when deposited in the brain even in small amounts, has also been shown to be toxic to humans, and is believed to cause neurodementia such as Parkinson's disease, Alzheimer's disease and dialysis encephalopathy, osteoporosis, etc [14]. In 1989, Al^{3+} was listed to be one of the food pollution sources [15]. The World Health Organization (WHO) recommends an average daily human intake of Al^{3+} of around 3–10 mg kg^{-1} and the tolerable weekly dietary intake as 7 mg kg^{-1} body weight [16]. Furthermore, nearly 40% of acidic soils worldwide are thought to be polluted because of the effects of aluminum toxicity, which is the critical factor that hinders crop production in acidic soils [17].

Conventional analytical techniques, including inductively coupled plasma-mass spectrometry (ICP-MS), liquid chromatography and atomic absorption spectrometry are mostly utilized for Fe^{3+} and Al^{3+} analysis. Advantages of these techniques are short response times and high sensitivity, whereas disadvantages include multistep processing and low selectivity [18]. Fluorescence sensing has gradually emerged as a significant and effective approach for the recognition of metal ions due to its simplicity, high sensitivity and instantaneous response [19]. Up to now, a number of colorimetric and fluorescent chemosensors for Al^{3+} or Fe^{3+} have been reported [20-28]. However, most of the reported fluorescent chemosensors can selectively sense only one of them. So, chemosensors with differential responses towards multiple ions are cost-effective and will win high praise from the viewpoint of practical applications. Furthermore, compared to the common transition metal ions, the detection of Al^{3+} has always been challenging and problematic due to the poor coordination ability. So, developing such sensors with Al^{3+} and Fe^{3+} ions recognition capability is a challenging task [29].

In the recognition mechanism of the materials which put the guest molecules into the interior of host materials, as a useful sensor, the host needs to bind to the distinctive guest molecule in preference to other competing species and it must register the binding event in an appropriate form. Besides, chemical and thermal stability of the host molecule is necessary. The required features for the host molecules make porous metal-organic frameworks (MOFs) an attractive choice for molecular sensing [30]. MOFs, as indicated by the name, are crystalline solids constructed *via* self-assembly of single metal cations (primary building unit or PBU) or metal clusters (secondary building unit or SBU) and organic ligands having multiple binding sites, forming one, two, or three dimensional extended coordination networks [31]. Because of the tremendous choices of metal nodes and organic linkers, the optical properties of MOFs can be engineered [32]. Recently, fluorescent sensors based on MOFs have been regarded as one of the most promising candidates for detecting metal ions owing to their high efficiency, low cost, and portability. An efficient strategy is to develop and design the MOFs with excellent fluorescent response to analytes [33]. The intrinsic porosities of the luminescent MOFs enable them

to reversibly adsorb and release guest molecules and to provide a platform for specific luminescent recognition of targets due to the host-guest interactions [34]. Moreover, the extent of sensitivity of the detection process is enhanced due to the confinement of the analytes within the large cavities of the MOF materials. Also, the analytes can interact with the pore surface of MOF compounds through the Lewis acidic or basic as well as coordinatively unsaturated metal sites [35]. Moreover, in the successful production of functional luminescent MOFs, amino-decorated metal-organic frameworks are fascinating. The amino group in a luminescent MOF could be used as a binding site to bind with metal ions [36].

In order to achieve the goal of rational design of the MOF with high sensitivity and selectivity for analytes, we prepared two organic ligands 2,5-bis(4-pyridyl)-3,4-diaza-2,4-hexadiene (4-bpdh) and amino-1,4-benzenedicarboxylate (NH$_2$-BDC) and employed it to react with Zn(II) salt to construct crystalline solid luminescent materials for a number of reasons: (1) Transition-metal ions, without unpaired electrons (such as Zn^{2+}-like has d^{10} formations), can gain linker-based highly emissive materials; (2) The rigidity of the two ligands can help to construct stable networks as well as the added flexibility and diversity in the geometric structure of MOF; (3) The NH$_2$ group in organic luminescent materials can be regarded as an electron-donating group suitable for binding the electron accepting metal ions. As a result, a microporous MOF, [Zn$_2$(NH$_2$-BDC)$_2$(4-bpdh)]·3DMF (TMU-16-NH$_2$) decorated with NH$_2$ and imine sites was successfully achieved under solvothermal conditions [37]. Furthermore, the fluorescent sensor properties for Al^{3+} and Fe^{3+} were presented and discussed in detail. The fluorescence studies show that TMU-16-NH$_2$ can sense Fe^{3+} and Al^{3+} through fluorescence quenching and enhancement, respectively. Especially, the selectivity to Fe^{3+} and Al^{3+} is not interfered by Na$^+$, K$^+$, Li$^+$, Cu^{2+}, Mg^{2+}, Ba^{2+}, Zn^{2+}, Cd^{3+}, Co^{2+}, Pb^{2+}, As^{3+}, Ni^{2+}, Mn^{2+}. More importantly, this MOF can realize fast detection for Fe^{3+} and Al^{3+} with a response time of less than 1 min, as well as showing low detection limits of 0.7 μM and 0.09 μM, respectively.

Experimental section

Chemicals, reagents and apparatus

Starting reagents for the synthesis were purchased and used without further purification from commercial suppliers (Sigma-Aldrich, Merck and others). Zn(NO$_3$)$_3$·6H$_2$O and amino-1,4-benzenedicarboxylic acid (NH$_2$-BDC) were used to synthesize TMU-16-NH$_2$. N,N-dimethylformamide (DMF) was used as the solvent to purify TMU-16-NH$_2$. Aqueous solutions of Cd^{2+}, Zn^{2+}, Pb^{2+}, Co^{2+}, As^{3+}, Mn^{2+}, Al^{3+}, Cu^{2+}, Ni^{2+} and Fe^{3+} were prepared from CdCl$_2$·2.5H$_2$O, Zn(NO$_3$)$_3$·6H$_2$O, Pb(NO$_3$)$_2$, Co(NO$_3$)$_2$·6H$_2$O, NaAsO$_2$, MnCl$_2$·6H$_2$O, Al(NO$_3$)$_3$·9H$_2$O, Cu(NO$_3$)$_2$·3H$_2$O, Ni(OAc)$_2$·4H$_2$O, and Fe(NO$_3$)$_3$·9H$_2$O, respectively. The infrared spectra were recorded on a Nicolet Fourier Transform IR, Nicolet 100 spectrometer in the range 500-4000 cm^{-1} using the KBr disk technique. X-ray powder diffraction (XRD) measurements were performed using a Philips X'pert diffractometer with monochromated Cu-k$_\alpha$ radiation (λ=1.54056Å). The simulated XRD powder pattern based on single crystal data was prepared using Mercury software [38]. Volumetric N$_2$ sorption isotherm were collected at 77 K using an ASAP 2020 HD (Micromeritics). Temperature was controlled by using a liquid nitrogen bath. The total pore volumes (V$_t$) were calculated at P/P$_0$ = 0.95. The fluorescence experiments were performed at room temperature on a Shimadzu RF-6000 fluorescence spectrometer (kyoto, Japan) with a photomultiplier voltage of 700 V, scan speed of 60,000 nm min^{-1}, excitation slit width of 900 nm, emission slit width of 200-800 nm, and a 380 nm optical filter. The fluorescent emission spectra were recorded in the wavelength range of 300-800 nm upon excitation at 360 nm.

Preparation of 2,5-bis(4-pyridyl)-3,4-diaza-2,4-hexadiene (4-bpdh)

The ligand 2,5-bis(4-pyridyl)-3,4-diaza-2,4-hexadiene (4- bpdh) was synthesized according

to previously reported methods [39]. 2.3 g (4.5 mmol) of hydrazine hydrate was added dropwise to a solution of 4- acetylpyridine (1.089 g, 9.0 mmol) dissolved in ethanol (15 mL). Two drops of formic acid were added and the mixture was stirred at room temperature for 24 h. The yellow solid that formed was filtered and washed several times with ethanol/ether (1:1). Yield: 0.536 g (50 %).

Preparation of [Zn₂(NH₂-BDC)₂(4-bpdh)]·3DMF (TMU-16-NH₂)

The TMU-16-NH₂ MOF was prepared following the published protocol [37]. Briefly, $Zn(NO_3)_2·6H_2O$ (0.297 g, 1 mmol), 4-bpdh (0.119 g, 0.5 mmol), NH₂-BDC (0.181 g, 1 mmol) were dissolved in 15 mL DMF. The mixture was placed in a Teflon reactor and heated at 80 °C for 3 days, and then it was gradually cooled to room temperature. The crystals were obtained in a 41% yield. IR (cm⁻¹): 3460.13 (s), 3348.32 (s), 1666.74 (vs), 1628.27 (vs), 1428.57 (vs), 1377.88 (vs), 1257.27 (s), 831.09 (s), 767.46 (s), 574.08 (s).

Luminescent experiments

The luminescence properties of TMU-16-NH₂ dispersed in DMF were investigated at room temperature. The suspension was prepared by introducing 1 mg of TMU-16-NH₂ power into 4 mL solvent then under ultrasonic agitation for 10 min. To a 1 cm × 1 cm quartz cell, a TMU-16-NH₂ suspension (250 mg L⁻¹, 4 mL), and certain amounts (20 µL) of selected analytes were sequentially added. The mixtures were then used for fluorescence measurements.

Results and discussion

Characterization of TMU-16-NH₂

The solvothermal reaction of the organic ligands NH₂-BDC and 4-bpdh with $Zn(NO_3)_2·6H_2O$ in *N,N*-dimethylformamide (DMF) afforded a three-dimensional (3D) structure of TMU-16-NH₂ (Figure 1a) [40]. TMU-16-NH₂ is composed of paddle-wheel dinuclear zinc carboxylate units which are bridged by the NH₂-BDC ligands to form a distorted 2D square grid. The 2D square grids are pillared by 4-bpdh molecules, whose nitrogen atoms occupy the axial sites of the [Zn₂(COO)₄] paddle wheels to form a 3D framework (Figure 1b, c). As a result, the pore surface of TMU-16-NH₂ is decorated with pendant amine and imine functional groups. Two of the 3D frameworks interpenetrate in TMU-16-NH₂, reducing the pore size. A 1D channel occurs in the direction of the rectangular diagonal of the paddle-wheel clusters (Figure 1d). This channel has a cross section of approximately 3 Å (including van der Waals radii), thus suggesting a microporous characteristic of TMU-16-NH₂.
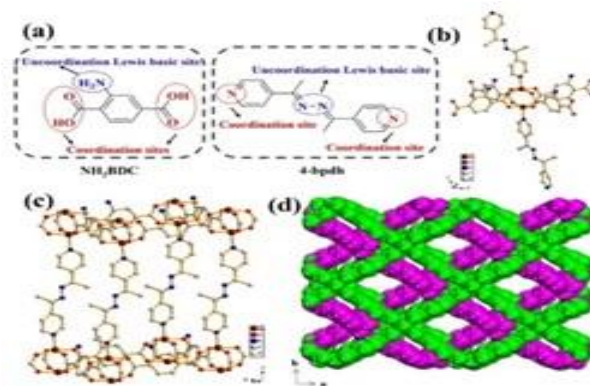

Figure 1. (a) Molecular structure of NH₂-BDC and 4-bpdh. (b) The coordination environments of Zn(II) ions in TMU-16-NH₂ . (c) An elongated primitive cubic net of TMU-16-NH₂ which contains 1D channels of 8 Å. (d) Representations of the two-fold interpenetration TMU-16-NH₂ which contain 1D channels of 3 Å, viewed along the rectangular diagonal of the paddle-wheel clusters. The two interpenetrating frameworks are shown in purple and green. All hydrogen atoms and the disordered guest molecules are omitted for clarity.

The experimental XRD pattern of the synthesized TMU-16-NH$_2$ was in good agreement with the simulated one, showing the successful preparation of TMU-16-NH$_2$ (Figure 2a). Interestingly, TMU-16-NH$_2$ exhibits a dynamic/flexible framework nature involving framework transformation and/or deformation, which has been widely observed in such 3D interpenetrated frameworks of primitive cubic nets [41-43]. When the as-synthesized TMU-16-NH$_2$ is immersed in different solvents such as EtOH, CH$_2$Cl$_2$, CH$_3$CN, CH$_3$Cl and toluene, it shows a slight change in d-spacing and the disappearance of a few peaks in the PXRD patterns (Figure 2a), which is a common phenomenon for the doubly interpenetrated MOFs as established by Kitagawa et al. [44-45].

For TMU-16-NH$_2$, the strong vibrations at 1666 and 1628 cm^{-1} correspond to the asymmetric stretching vibration of the –COO$^-$ group, whereas its symmetric stretching vibrations appear at 1428 and 1377 cm^{-1} (Figure 2b). The difference of frequency between asymmetric and symmetric stretching vibration is more than 200 cm^{-1} indicating the bidentate-bridging coordination mode of the –COO$^-$ group [46]. The as-prepared TMU-16-NH$_2$ was also monitored by TG analysis. TGA data indicate that TMU-16-NH$_2$ releases its guest molecules over the temperature ranges 25-230 °C to form the guest-free phases, [Zn$_2$(NH$_2$-BDC)$_2$(4-bpdh)] (Figure 2c). Weight losses of about 23% were measured for the MOF, which is attributed to the loss of 3DMF (calc.: ~24%). The network TMU-16-NH$_2$ is thermally stable up to 320 °C as evidenced by the fact that no additional weight loss was observed at those temperatures, implying the good thermal stability of this MOF. The porosity of TMU-16-NH$_2$ was also characterized by the N$_2$ adsorption isotherm at 77 K in Figure 2d. The BET specific surface area of TMU-16-NH$_2$ showed a characteristic type I behavior of microporous materials, as expected from its crystal structure (BET area (A$_{BET}$) = 103 m^2 g^{-1}; pore volume (V$_t$) = 0.09 cm^3 g^{-1}).
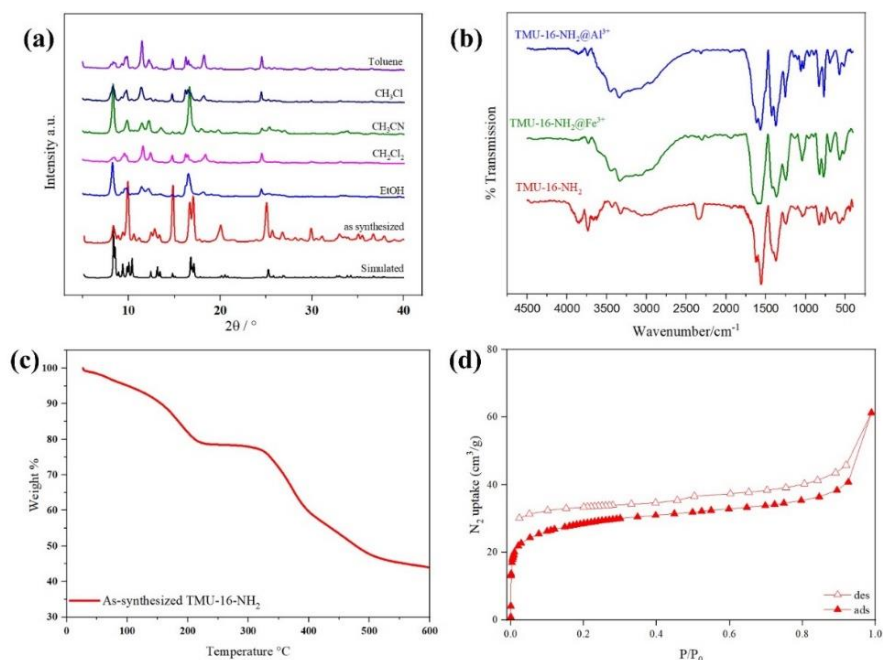

Figure 2. (a) PXRD of TMU-16-NH$_2$: simulated (black), as-synthesized (red); immersed in EtOH (blue), CH$_2$Cl$_2$ (pink), CH$_3$CN (green), CH$_3$Cl (dark blue), and Toluene (purple). (b) FT-IR spectra of TMU-16-NH$_2$ (red), TMU-16-NH$_2$@Fe^{3+} (green) and TMU-16-NH$_2$@Al^{3+} (blue) (c) TGA of as-synthesized TMU-16-NH$_2$. (d) Nitrogen adsorption–desorption isotherms of TMU-16-NH$_2$ at 77 K

Fluorescent properties of TMU-16-NH₂

Previous studies have shown that d^{10} coordination polymers containing zinc(II) may exhibit photoluminescence properties [47]. The most significant structural feature of TMU-16-NH₂ is the presence of free amine and imine sites within the pores, highlighting the potential for its recognition of metal ions and thus for sensing functions. First of all, the emission spectra of TMU-16-NH₂ in DMF solution were measured at different excitation wavelength and are shown in Figure 3a. The emission wavelength is nearly excitation-independent, with the maximum excitation wavelength and the maximum emission wavelength at 360 and 440 nm, respectively. Moreover, as shown in Figure 3b, when TMU-16-NH₂ was dispersed in DMF solution it has an emission peak at 440 nm with a weak luminescent intensity, which is approximately four times lower than the ligand NH₂-BDC dispersed in DMF. This interesting phenomenon can be attributed to the ligand-to-metal charge transfer (LMCT) effect upon the ligand NH₂-BDC coordination with Zn-O clusters to form the TMU-16-NH₂ framework.

Furthermore, the solvent induced luminescence quenching effect may also play an important role in weakening the luminescent intensity of TMU-16-NH₂ in DMF solution, which was mainly dependent on the polarity of solvent molecules and their coupling with the Zn-O nodes as reported [48].

Furthermore, we also examined the luminescence properties of TMU-16-NH₂ MOF in different solvent emulsions. Compound TMU-16-NH₂ (1 mg) was dispersed in different commonly used organic solvents (4 mL) like ethanol (EtOH), methanol (MeOH), N,N′-dimethylformamide (DMF), tetrahydrofuran (THF), dichloromethane (CH₂Cl₂) and acetonitrile (MeCN). As shown in Figure 3c, the PL intensity is largely dependent on the solvent molecules, particularly in the case of MeOH, which exhibited the most significant enhancing effects. Shifts in emission are observed upon changing the solvent, and the wavelength corresponding to the maximum peak decreases in the order MeOH > DMF > EtOH > CH₂Cl₂ > CH₃CN > THF (Figure 3d).
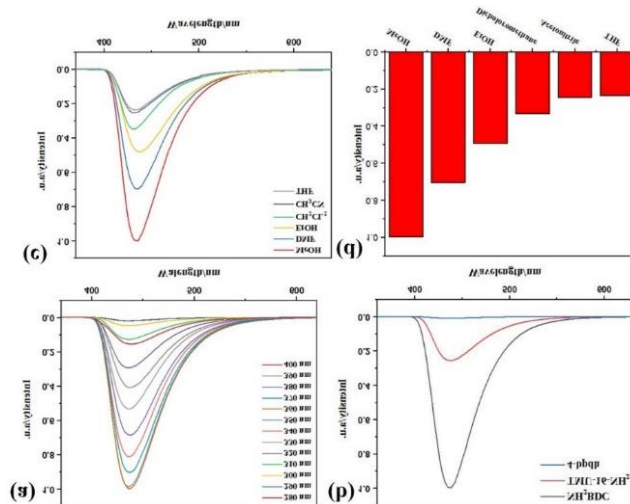
EtOH > CH₂Cl₂ > CH₃CN > THF (Figure 3d).

Figure 3. (a) Photoluminescence emission spectra (with progressively longer excitation wavelengths from 280 nm to 400 nm) of TMU-16-NH₂. (b) The PL spectra of TMU-16-NH₂ (red), NH₂-BDC (black) and 4-bpdh (blue) suspensions in DMF. (c) The PL spectra of TMU-16-NH₂-solvent emulsions at room temperature, where the red, blue, yellow, green, purple, green and gray curves denote the intensities of TMU-16-NH₂-MeOH, -DMF, -EtOH, -CH₂Cl₂, -CH₃CN, and -THF, respectively. (d) Comparisons of the luminescence intensity of TMU-16-NH₂-solvent emulsions at room temperature

To examine the potential of TMU-16-NH$_2$ for sensing of metal ions, the as-synthesized samples (1 mg) were ground and immersed in DMF solutions (4 mL) containing different metal ions (Zn^{2+}, Pb^{2+}, Co^{2+}, Cu^{2+}, Cd^{2+}, Al^{3+}, Fe^{3+}, As^{3+}, Mn^{2+} and Ni^{2+}) to form a metal-ion-incorporated MOF suspension. To ensure the consistency of experimental conditions, the solution was mixed for 30 min before the collection time of fluorescence data. The luminescent spectra were recorded and are compared in Figure 4. The emission spectra show that the various metal ions display markedly different effects on the luminescence of the MOF, particularly for Fe^{3+} ion and Al^{3+} ion, whose varying extents could be easily distinguished. The incorporation of Fe^{3+} ion into the MOF system could drastically quench the emission of TMU-16-NH$_2$, whereas the emission could be greatly enhanced after addition of the Al^{3+} ion. Other metal ions only show little or mild effect (for Zn^{2+} and Cd^{2+} ions) on the luminescent intensity of the TMU-16-NH$_2$. Such a character might be useful for the detection of targeted metal ion such as Al^{3+} or Fe^{3+} ions [49].
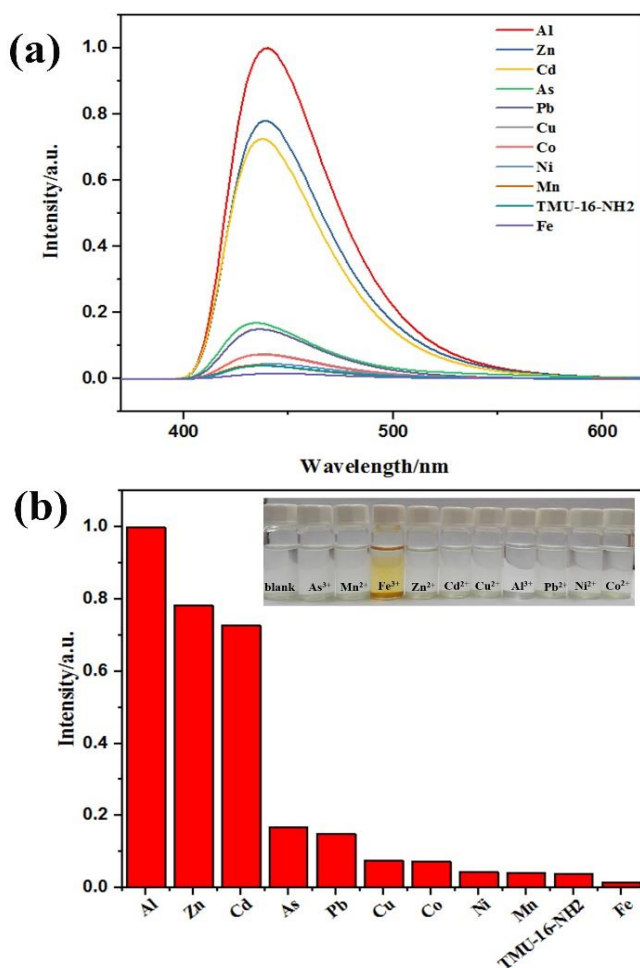

Figure 4. (a) Fluorescence spectra and (b) relative room-temperature luminescence intensities of TMU-16-NH$_2$ (1 mg) at 440 nm in DMF suspension (4 mL) upon addition of various metal ions (20 µL; excited at 360 nm). (Inset: photographs of M^{n+}@TMU-16-NH$_2$ sample in DMF)

To explore the fluorescence quenching and enhancement further, the detailed studies of the luminescence properties of TMU-16-NH$_2$ in the presence of Fe^{3+} and Al^{3+} ions were carried out. To validate the high selectivity of TMU-16-NH$_2$ for detection of Fe^{3+} and Al^{3+}, competition experiments have been carried out to evaluate the efficiency of TMU-16-NH$_2$ towards Fe^{3+} and Al^{3+} ions by recording its luminescent intensity in the presence of equal concentration of the interference metal ions such as Zn^{2+}, Cd^{2+}, K$^+$, Ba^{2+}, Mg^{2+}, Cu^{2+}, Na$^+$, As^{3+}, Pb^{2+}, Co^{2+}, Ni^{2+}, Mn^{2+} and Li$^+$. Upon the introduction of Fe^{3+} to the mixture of TMU-16-NH$_2$ and other metal cations, the fluorescence is significantly quenched (Figure 5a). Similarly, when Al^{3+} was introduced to the mixture of TMU-16-NH$_2$ and other metal cations, the fluorescence of the ligand is significantly enhanced (Figure 5b). This reveals that the interference from conventional metal cations can be neglected, further confirming the high selectivity of TMU-16-NH$_2$ for Fe^{3+} and Al^{3+} detection and the potential of TMU-16-NH$_2$ for practical use.
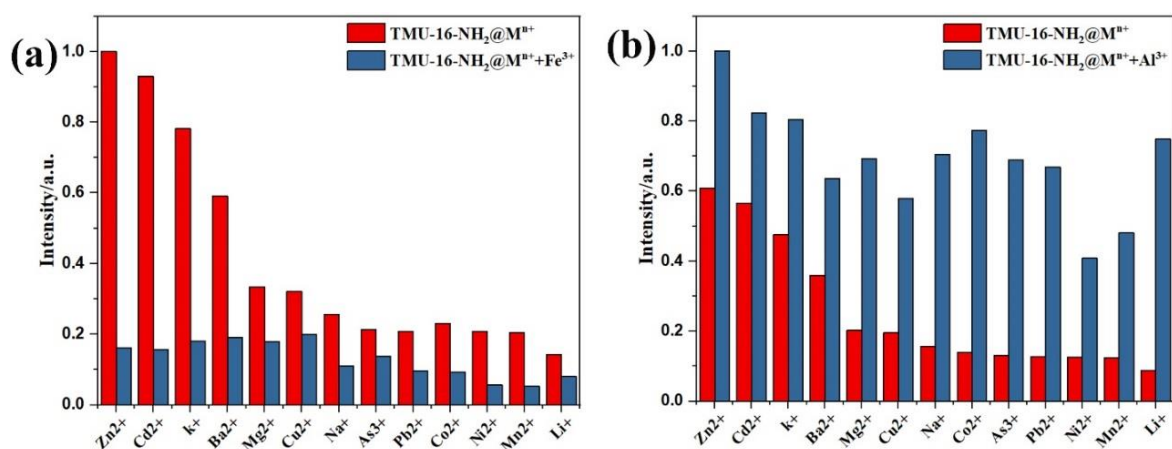

Figure 5. Comparison of the luminescence intensity of TMU-16-NH$_2$ with (a) 100 μM Fe^{3+} and (b) 100 μM Al^{3+} in DMF in presence of 100 μM of other metal ions, monitored at 440 nm. (Red: Competing ions; Blue: Competing ions + Fe^{3+} or Al^{3+})

To better understand the fluorescence response of TMU-16-NH$_2$ to Fe^{3+} and Al^{3+}, concentration-dependent luminescence measurements were also carried out. The as-synthesized TMU-16-NH$_2$ solid samples were ground and immersed in different concentrations of Fe^{3+} and Al^{3+}, and then their luminescence spectra were recorded. As demonstrated in Figure 6a and b, the emission intensity of the TMU-16-NH$_2$ suspension at 440 nm was quenched steadily with increasing Fe^{3+} concentration and enhanced accordingly with increasing Al^{3+} concentration. As demonstrated in Figure 6c and e, when the Fe^{3+} concentration increased from 0 to 450 μM, the emission intensity of TMU-16-NH$_2$ was gradually decreased and a good linear relationship (correlation coefficient R = 0.994) between the emission intensity of TMU-16-NH$_2$ and the concentration of Fe^{3+} was observed in the range of 0-250 μM of Fe^{3+}. On the other hand, when the Al^{3+} concentration increased from 0 to 550 μM, the emission intensity of the MOF was gradually increased and a good linear relationship (R = 0.999) between the emission intensity of TMU-16-NH$_2$ and the concentration of Al^{3+} was observed in the range of 0-150 μM of Al^{3+} (Figure 6d, f).

The fluorescence quenching and enhancing follow the Stern–Völmer (SV) equation: $I_0/I = 1 + K_{SV}[M]$, where I_0 and I correspond to the luminescence intensity for TMU-16-NH$_2$ in absence and presence of metal cations, respectively, [M] is the metal concentration, and

K_{SV} is the Stern–Völmer constant. It is thus expected that the reduction or increase in luminescence intensity is proportional to the concentration of the metal ions. It was found that the SV plot of TMU-16-NH$_2$ towards both Fe^{3+} and Al^{3+} ions is nearly linear at low concentration range, but subsequently deviates from linearity and bends upwards at higher concentrations (Figure 6c, d). The K_{SV} values are calculated *via* luminescent data. An exceptionally high K_{SV} value of 21600 M^{-1} was obtained for Fe^{3+}, while K_{SV} for Al^{3+} was 1435 M^{-1}. Obviously, TMU-16-NH$_2$ shows highly selective sensing for both Fe^{3+} and Al^{3+} ions (Figure 6e, f). The sensitivity of TMU-16-NH$_2$ is equal or higher than that for previously reported MOFs with K_{SV} values in the range of tens to hundreds M^{-1}

(Tables 1 and 2). The high sensitivity allows us to easily identify the existence of a small amount of Fe^{3+} and Al^{3+} ions.

To further corroborate the high sensitivity of TMU-16-NH$_2$ compared to other reported systems, we determined the detection limit for Fe^{3+} and Al^{3+} on the basis of the 3δ IUPAC criterion [50-51]. Based on the slope of the calibration curve (K) values and the standard deviations (S$_b$) from ten repeated fluorescent measurements of blank solutions, the detection limits (3S$_b$/K) of TMU-16-NH$_2$ towards Fe^{3+} ion in DMF were calculated to be 0.7 μM (corresponding to 40 ppb) and 0.09 μM (2.4 ppb) for Al^{3+}. This is also comparable to or better than some previously reported Fe^{3+} and Al^{3+} fluorescent sensors (Tables 1 and 2).
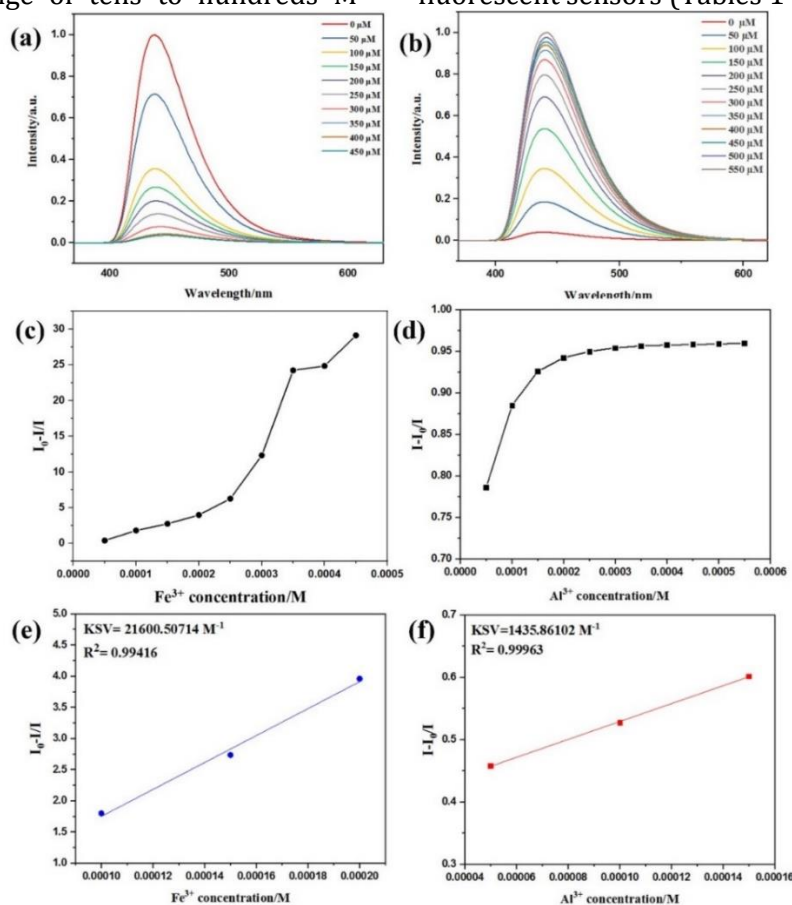

Figure 6. The luminescence spectra of TMU-16-NH$_2$ with different concentration of (a) Fe^{3+} and (b) Al^{3+} ions. Stern-Völmer (SV) plots of the fluorescence emissions of TMU-16-NH$_2$ quenched by (c) Fe^{3+} and (d) Al^{3+} ions in DMF with 360 nm excitation (emission decays were monitored at 440 nm) SV plots of the fluorescence emissions of TMU-16-NH$_2$ quenched or enhanced by (e) Fe^{3+} and (f) Al^{3+} ions, respectively.

Table 1. TMU-16-NH$_2$ sensing parameter comparison with other MOF based Fe^{3+} sensors

MOF	Medium	K$_{SV}$ (M^{-1})	Detection limit (µM)	Line range	Ref
Eu^{3+}@MIL-53-COOH (Al)	H$_2$O	5.12×10^3	0.5	0-0.5 mM	[52]
BUT-15	H$_2$O	1.66×10^4	0.8	20-700 µM	[53]
BUT-14	H$_2$O	2.17×10^3	3.8	20-700 µM	[53]
[Cd(L)(BPDC)]	H$_2$O	3.63×10^4	2.21	0.0025-0.15 mM	[54]
[Cd(L)(SDBA)(H$_2$O)]	H$_2$O	3.59×10^4	7.14	0.0025-0.15 mM	[54]
[Cd(ATA)(L)]	H$_2$O	3.838×10^3	1.77	0-2 mM	[55]
[Zn(ATA)(L)]	H$_2$O	0.557×10^3	3.76	0-2 mM	[55]
[Eu(HL)(DMF)(H$_2$O)$_2$]	H$_2$O	1.519×10^3	_	0-5 mM	[56]
[Tb(HL)(DMF)(H$_2$O)$_2$]	H$_2$O	4.479×10^3	50	0-5 mM	[56]
[Eu(L)(BPDC)$_{1/2}$(NO$_3$)]	DMF	5.16×10^4	0.5	-	[57]
[Tb(L)(BPDC)$_{1/2}$(NO$_3$)]	DMF	4.30×10^4	0.5	-	[57]
[Cd(5-asba)(bimb)]	H$_2$O	1.78×10^4	0.0061	0.01875-0.225 mM	[58]
[Eu$_2$K$_2$(dcppa)$_2$(H$_2$O)$_6$]		4.3×10^4	1	10^{-6}-10^{-2} M	[4]
TMU-16-NH$_2$	DMF	2.16×10^4	0.7	50-700 µM	In work

Table 2. TMU-16-NH$_2$ sensing parameter comparison with other Al^{3+} sensors

Sensor	Medium	Detection limit (ppb)	Line range	Ref
nitrogen-doped carbon quantum dot	DMF-water	0.7		[5]
[Cd$_2$(syn-dftpmcp)(1,3 BDC)$_2$]	CH$_3$CN	183 ppb	0.01–0.05 ppm	[59]
Zn(HTABDC)(Bpy)·DMF	H$_2$O	3.73 ppb		[60]
IRMOF-3	EtOH	267 ppb	0-0.13 mM	[48]
[Co$_2$(dmimpym)(nda)$_2$]	DMF	0.7		[46]
[Co(OBA)-(DATZ)$_{0.5}$(H$_2$O)]	H$_2$O	57.5 ppb		[61]
TMU-16-NH$_2$	DMF	0.094	50-150 µM	In work

Additionally, to investigate the time-response characteristic of the TMU-16-NH$_2$ sensor toward Fe^{3+} and Al^{3+} ions, the fluorescence intensity of TMU-16-NH$_2$ (λ_{ex} = 360 nm) was measured as a

function of immersion time in DMF solutions of 100 μM metal ions (Figure 7). With increasing time, the PL intensity decreases for the Fe^{3+}-loaded sample and increases for the Al^{3+}-loaded MOF. Both of the metal ions show very fast fluorescence quenching/enhancing reaction. The emission intensities of TMU-16-NH$_2$ at 440 nm have been decreased/increased to more than 2.3 and 2.8 times in less than 1 min for Fe^{3+} and Al^{3+} ions, respectively, and constant values in about 2 min (Figure 7a, b). This response is much faster than that in the some previous reports (about 24 h or 72 h). This rapid response is quite appealing and may be attribute to the fact that Fe^{3+} and Al^{3+} ions can rapidly diffuse into the channels of TMU-16-NH$_2$ and interact with luminophores on the pore surface.

Besides the sensitivity and selectivity of luminescent materials in detecting analytes, the reusability of the materials is also very important for practical applications. Therefore, we also explored the reusability of the TMU-16-NH$_2$ probe towards Fe^{3+} and Al^{3+} ions up to four cycles. For checking its reusability, the MOF compound was filtered off after each fluorescence titration experiment. The filtered materials were washed with DMF repeatedly and then dried in an oven. TMU-16-NH$_2$ showed outstanding recovery of its initial fluorescence intensity, even after four consecutive cycles of fluorescence sensing experiments, demonstrating its good recyclability and stability for the detection applications (Figure 7c, d).
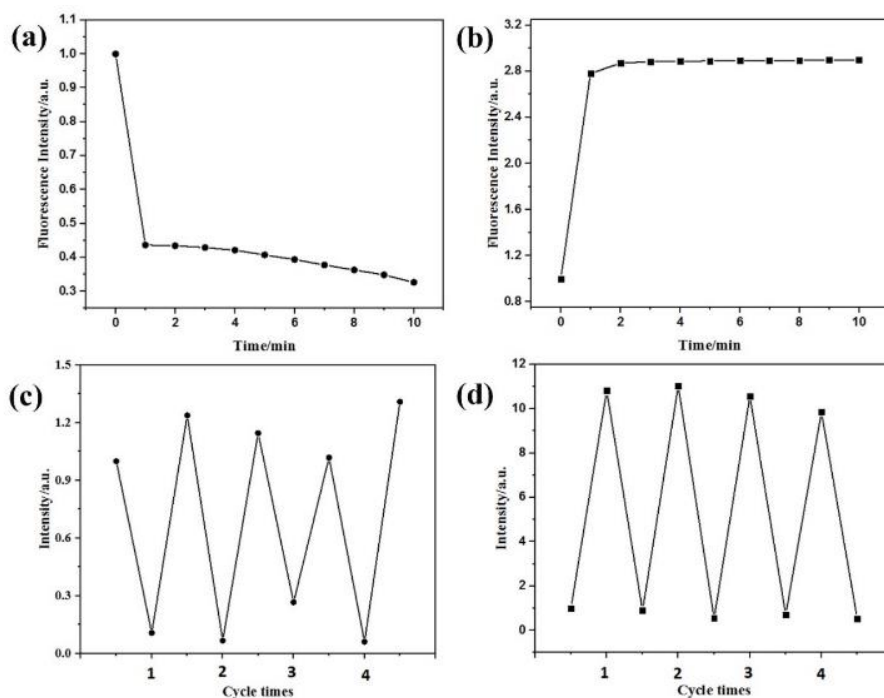

Figure 7. Fluorescence quenching and enhancement of TMU-16-NH$_2$ by (a) 100 μM Fe^{3+} and (b) 100 μM Al^{3+}, respectively, in DMF as a function of time (λ_{ex}= 360 nm). Recovery tests of TMU-16-NH$_2$ for (c) 100 μM Fe^{3+} and (d) 100 μM Al^{3+} in DMF.

According to the previous reports, the quenching or enhancing effects on luminescence MOFs by metal cations may be attributed to the following factors: (a) interactions between metal cations and organic ligands; (b) collapse of the crystal structure by the metal cations; (c) cation exchange between the central cations of the frameworks and the targeted cations .The quick response time as well as the recoverable character implies the luminescent quenching should not be attributed to the neither cation exchange nor collapse of the crystal structure.

Furthermore, the PXRD measurements were carried out to study the metal ion incorporated MOF samples of TMU-16-NH$_2$@M^{n+}. As shown in Figure 8, the PXRD patterns of the TMU-16-NH$_2$@M^{n+} show a slight change in d-spacing and the disappearance of a few peaks, which could be attributed to the flexible nature of the framework [43]. Moreover, an examination of the FT-IR spectra of TMU-16-NH$_2$ and Fe^{3+}/Al^{3+} immersed TMU-16-NH$_2$ showed the peaks in TMU-16-NH$_2$@M^{n+} to be broadened and slightly red-shifted with respect to those of the pure

crystals of TMU-16-NH$_2$ (Figure 2b), suggesting interactions of metal ions with the host framework. According to the reported literature, porous MOFs with Lewis basic sites, such as amine, pyridyl, amide and anionic sulfonate sites, can have significant interactions with guest metal ions [62-63]. We therefore suggest that the quenching/enhancing might be related to the interaction between the Fe^{3+}/Al^{3+} ions and pendant amine and imine functional groups in TMU-16-NH$_2$.
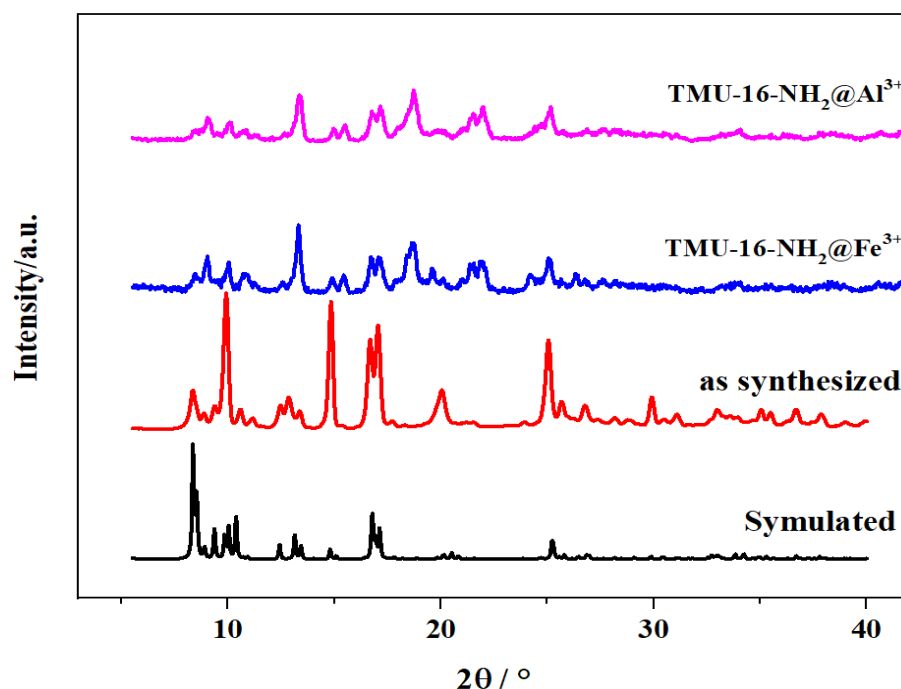

Figure 8. PXRD of TMU-16-NH$_2$: simulated (black), as-synthesized (red), TMU-16-NH$_2$@Fe^{3+} (blue) and TMU-16-NH$_2$@Al^{3+} (pink

Conclusion

In this work, we have reported the synthesis and metal ions sensing properties of amine/imine-functionalized microporous TMU-16-NH$_2$ MOF. TMU-16-NH$_2$ could be employed as potential multifunctional luminescent material for sensing of Fe^{3+} and Al^{3+} ions with high selectivity and considerable sensitivity and fast response time. The limit of detection of this luminescent

probe for Fe^{3+}/Al^{3+} in DMF medium was found to be 0.7 μM and 0.09 μM respectively, which is comparable to the recommended maximum contaminant level or to the value mentioned in the guidelines of WHO for Fe^{3+} (0.3mg/L, 5.4 μM) and Al^{3+} (0.2 mg/L, 7.4 μM) in drinking water. Based on the experimental results, Lewis basic sites within porous MOFs are expected to play very important roles for their recognition of Lewis acidic metal ions, and thus to find

functionalities in chemical transformation and sensing. The present results may provide a facile route to design and synthesize functional MOFs with applications in fluorescent sensors for chemical, environmental and biological systems.

Acknowledgements

References

[1] D.W. Domaille, E.L. Que, C.J. Chang, *Nat. Chem. Biol.,* **2008**, *4*, 168-175. [Crossref], [Google Scholar], [Publisher]

[2] N.R. Chereddy, P. Nagaraju, M.N. Raju, V.R. Krishnaswamy, P.S. Korrapati, P.R. Bangal, V.J. Rao, *Biosens. Bioelectron.,* **2015**, *68*, 749-756. [Crossref], [Google Scholar], [Publisher]

[3] D. Zhao, X.-H. Liu, Y. Zhao, P. Wang, Y. Liu, M. Azam, S.I. Al-Resayes, Y. Lu, W.-Y. Sun, *J. Mater. Chem., A* **2017**, *5*, 15797-15807. [Crossref], [Google Scholar], [Publisher]

[4] H. Zhang, R. Fan, W. Chen, J. Fan, Y. Dong, Y. Song, X. Du, P. Wang, Y. Yang, *Cryst. Growth Des.,* **2016**, *16*, 5429-5440. [Crossref], [Google Scholar], [Publisher]

[5] T.-T. Xu, J.-X. Yang, J.-M. Song, J.-S. Chen, H.-L. Niu, C.-J. Mao, S.-Y. Zhang, Y.-H. Shen, *Sens. Actuator B-Chem,* **2017**, *243*, 863-872. [Crossref], [Google Scholar], [Publisher]

[6] H. Zhang, Y. Chen, M. Liang, L. Xu, S. Qi, H. Chen, X. Chen, *Anal. Chem.,* **2014**, *86*, 9846-9852. [Crossref], [Google Scholar], [Publisher]

[7] X.-H. Yang, S. Li, Z.-S. Tang, X.-D. Yu, T. Huang, Y. Gao, *Chin. Chem. Lett.,* **2015**, *26*, 129-132. [Crossref], [Google Scholar], [Publisher]

[8] V.K. Gupta, N. Mergu, L.K. Kumawat, *Sens. Actuator B-Chem,* **2016**, *223*, 101-113. [Crossref], [Google Scholar], [Publisher]

[9] M. Zheng, H. Tan, Z. Xie, L. Zhang, X. Jing, Z. Sun, *ACS Appl. Mater. Interfaces,* **2013**, *5*, 1078-1083. [Crossref], [Google Scholar], [Publisher]

[10] S. Goswami, S. Paul, A. Manna, *RSC Adv.,* **2013**, *3*, 10639-10643. [Crossref], [Google Scholar], [Publisher]

[11] V.N. Mehta, R.K. Singhal, S.K. Kailasa, *RSC Adv.,* **2015**, *5*, 33468-33477. [Crossref], [Google Scholar], [Publisher]

[12] S.V. Verstraeten, L. Aimo, P.I. Oteiza, *Arch. Toxicol.,* **2008**, *82*, 789-802. [Crossref], [Google Scholar], [Publisher]

[13] S. Gui, Y. Huang, F. Hu, Y. Jin, G. Zhang, L. Yan, D. Zhang, R. Zhao, *Anal. Chem.,* **2015**, *87*, 1470-1474. [Crossref], [Google Scholar], [Publisher]

[14] J. Wang, Y. Pang, *RSC Adv.,* **2014**, *4*, 5845-5848. [Crossref], [Google Scholar], [Publisher]

[15] X. Mu, L. Qi, J. Qiao, H. Ma, *Anal. Methods*, **2014**, *6*, 6445-6451. [Crossref], [Google Scholar], [Publisher]

[16] E. Özcan, S.O. Tümay, H.A. Alidağı, B. Çoşut, S. Yeşilot, *Dyes and Pigments*, **2016**, *132*, 230-236. [Crossref], [Google Scholar], [Publisher]

[17] H. Kim, B.A. Rao, J.W. Jeong, S. Mallick, S.-M. Kang, J.S. Choi, C.-S. Lee, Y.-A. Son, *Sens. Actuator B-Chem*, **2015**, *210*, 173-182. [Crossref], [Google Scholar], [Publisher]

[18] M. Zhang, J. Han, H. Wu, Q. Wei, G. Xie, S. Chen, S. Gao, *RSC Adv.,* **2016**, *6*, 94622-94628. [Crossref], [Google Scholar], [Publisher]

[19] T. Liu, Y. Dong, X. Wan, W. Li, Y. Yao, *RSC Adv.,* **2015**, *5*, 76939-76942. [Crossref], [Google Scholar], [Publisher]

[20] Y.-W. Wang, M.-X. Yu, Y.-H. Yu, Z.-P. Bai, Z. Shen, F.-Y. Li, X.-Z. You, *Tetrahedron Lett.,* **2009**, *50*, 6169-6172. [Crossref], [Google Scholar], [Publisher]

[21] C.R. Lohani, J.-M. Kim, S.-Y. Chung, J. Yoon, K.-H. Lee, *Analyst*, **2010**, *135*, 2079-2084. [Crossref], [Google Scholar], [Publisher]

[22] F. K.-W. Hau, X. He, W.H. Lam, V. W.-W. Yam, *ChemComm*, **2011**, *47*, 8778-8780. [Crossref], [Google Scholar], [Publisher]

[23] X. Li, J. Chen, E. Wang, *Chin. J. Chem. Phys.,* **2014**, *32*, 429-433. [Crossref], [Google Scholar], [Publisher]

[24] C. Liang, W. Bu, C. Li, G. Men, M. Deng, Y. Jiangyao, H. Sun, S. Jiang, *Dalton Tran.,* **2015**, *44*, 11352-11359. [Crossref], [Google Scholar], [Publisher]

[25] W.-H. Ding, W. Cao, X.-J. Zheng, D.-C. Fang, W.-T. Wong, L.-P. Jin, *Inorg. Chem.,* **2013**, *52*, 7320-7322. [Crossref], [Google Scholar], [Publisher]

[26] X. Gao, Y. Lu, S. He, X. Li, W. Chen, *Anal. Chem. Acta*, **2015**, *879*, 118-125. [Crossref], [Google Scholar], [Publisher]

[27] N.R. Chereddy, S. Thennarasu, A.B. Mandal, *Dalton Trans.,* **2012**, *41*, 11753-11759. [Crossref], [Google Scholar], [Publisher]

[28] S. Goswami, S. Das, K. Aich, D. Sarkar, T.K. Mondal, C.K. Quah, H.-K. Fun, *Dalton Trans.,* **2013**, *42*, 15113-15119. [Crossref], [Google Scholar], [Publisher]

[29] Y. Chen, Y. Mi, Q. Xie, J. Xiang, H. Fan, X. Luo, S. Xia, *Anal. Methods*, **2013**, *5*, 4818-4823. [Crossref], [Google Scholar], [Publisher]

[30] S. Liu, Z. Xiang, Z. Hu, X. Zheng, D. Cao, *J. Mater. Chem.*, **2011**, *21*, 6649-6653. [Crossref], [Google Scholar], [Publisher]

[31] Z. Hu, B.J. Deibert, J. Li, *Chem. Soc. Rev.,* **2014**, *43*, 5815-5840. [Crossref], [Google Scholar], [Publisher]

[32] S. Sen, T. Mukherjee, B. Chattopadhyay, A. Moirangthem, A. Basu, J. Marek, P. Chattopadhyay, *Analyst*, **2012**, *137*, 3975-3981. [Crossref], [Google Scholar], [Publisher]

[33] X. Luo, X. Zhang, Y. Duan, X. Wang, J. Zhao, *Dalton Trans.,* **2017**, *46*, 6303-6311. [Crossref], [Google Scholar], [Publisher]

[34] D. Zhao, Y. Cui, Y. Yang, G. Qian, *CrystEngComm*, **2016**, *18*, 3746-3759. [Crossref], [Google Scholar], [Publisher]

[35] S. Mostakim, S. Biswas, *CrystEngComm*, **2016**, *18*, 3104-3113. [Crossref], [Google Scholar], [Publisher]

[36] R. Lv, J. Wang, Y. Zhang, H. Li, L. Yang, S. Liao, W. Gu, X. Liu, *J. Mater. Chem. A*, **2016**, *4*, 15494-15500. [Crossref], [Google Scholar], [Publisher]

[37] V. Safarifard, A. Morsali, *CrystEngComm,* **2014**, *16*, 8660-8663. [Crossref], [Google Scholar], [Publisher]

[38] M.C.S. Visualisation, Exploration and Analysis Made Easy. *The Cambridge Crystallographic Data Centre.* 2019 [Publisher]

[39] A.R. Kennedy, K.G. Brown, D. Graham, J.B. Kirkhouse, M. Kittner, C. Major, C. J. McHugh, P. Murdoch, W.E. Smith, *New J. Chem.,* **2005**, *29*, 826-832. [Crossref], [Google Scholar], [Publisher]

[40] V. Safarifard, A. Morsali, *Ultrason. Sonochem.,* **2018**, *40*, 921-928. [Crossref], [Google Scholar], [Publisher]

[41] B. Chen, C. Liang, J. Yang, D.S. Contreras, Y.L. Clancy, E.B. Lobkovsky, O.M. Yaghi, S. Dai, *Angew. Chem. International Edition*, **2006**, *45*, 1390-1393. [Crossref], [Google Scholar], [Publisher]

[42] B. Chen, S. Ma, F. Zapata, E.B. Lobkovsky, J. Yang, *Inorg. Chem.,* **2006**, *45*, 5718-5720. [Crossref], [Google Scholar], [Publisher]

[43] M.C. Das, H. Xu, S. Xiang, Z. Zhang, H.D. Arman, G. Qian, B. Chen, *Chem. Eur. J.,* **2011**, *17*, 7817-7822. [Crossref], [Google Scholar], [Publisher]

[44] S. Kitagawa, R. Kitaura, S.-I. Noro, *Angew. Chem. International Edition*, **2004**, *43*, 2334-2375. [Crossref], [Google Scholar], [Publisher]

[45] R. Kitaura, K. Fujimoto, S.-I. Noro, M. Kondo, S. Kitagawa, *Angew. Chem.,* **2002**, *114*, 141-143. [Crossref], [Google Scholar], [Publisher]

[46] W.-M. Chen, X.-L. Meng, G.-L. Zhuang, Z. Wang, M. Kurmoo, Q.-Q. Zhao, X.-P. Wang, B. Shan, C.-H. Tung, D. Sun, *J. Mater. Chem. A*, **2017**, *5*, 13079-13085. [Crossref], [Google Scholar], [Publisher]

[47] M. Allendorf, C. Bauer, R. Bhakta, R. Houk, *Chem. Soc. Rev.,* **2009**, *38*, 1330-1352. [Crossref], [Google Scholar], [Publisher]

[48] M. Wang, L. Guo, D. Cao, *Sens. Actuator B-Chem*, **2018**, *256*, 839-845. [Crossref], [Google Scholar], [Publisher]

[49] D.-M. Chen, N.-N. Zhang, C.-S. Liu, M. Du, *J. Mater. Chem. C*, **2017**, *5*, 2311-2317. [Crossref], [Google Scholar], [Publisher]

[50] G.L. Long, J.D. Winefordner, *Anal. Chem.,* **1983**, *55*, 712A-724A. [Crossref], [Google Scholar], [Publisher]

[51] S.A.A. Razavi, M.Y. Masoomi, A. Morsali, *Inorg. Chem.*, **2017**, *56*, 9646-9652. [Crossref], [Google Scholar], [Publisher]

[52] Y. Zhou, H.-H. Chen, B. Yan, *J. Mater. Chem. A*, **2014**, *2*, 13691-13697. [Crossref], [Google Scholar], [Publisher]

[53] B. Wang, Q. Yang, C. Guo, Y. Sun, L.-H. Xie, J.-R. Li, *ACS Appl. Mater. Interfaces*, **2017**, *9*, 10286-10295. [Crossref], [Google Scholar], [Publisher]

[54] S. Chen, Z. Shi, L. Qin, H. Jia, H. Zheng, *Cryst. Growth Des.,* **2016**, *17*, 67-72. [Crossref], [Google Scholar], [Publisher]

[55] B. Parmar, Y. Rachuri, K.K. Bisht, E. Suresh, *Inorg. Chem.,* **2017**, *56*, 10939-10949. [Crossref], [Google Scholar], [Publisher]

[56] S.T. Zhang, J. Yang, H. Wu, Y.Y. Liu, J.F. Ma, *Chem. Eur. J.,* **2015**, *21*, 15806-15819. [Crossref], [Google Scholar], [Publisher]

[57] W. Yan, C. Zhang, S. Chen, L. Han, H. Zheng, *ACS Appl. Mater. Interfaces*, **2017**, *9*, 1629-1634. [Crossref], [Google Scholar], [Publisher]

[58] Y.-J. Yang, M.-J. Wang, K.-L. Zhang, *J. Mater. Chem. C*, **2016**, *4*, 11404-11418. [Crossref], [Google Scholar], [Publisher]

[59] W.-X. Li, J.-H. Gu, H.-X. Li, M. Dai, D.J. Young, H.-Y. Li, J.-P. Lang, *Inorg. Chem.*, **2018**, 57, 13453-13460. [Crossref], [Google Scholar], [Publisher]

[60] Q. Li, X. Wu, X. Huang, Y. Deng, N. Chen, D. Jiang, L. Zhao, Z. Lin, Y. Zhao, *ACS Appl. Mater. Interfaces*, **2018**, *10*, 3801-3809. [Crossref], [Google Scholar], [Publisher]

[61] D. K. Singha, P. Mahata, *Inorg. Chem.*, **2015**, *54*, 6373-6379. [Crossref], [Google Scholar], [Publisher]

[62] J.-R. Li, R. J. Kuppler, H.-C. Zhou, *Chem. Soc. Rev.,* **2009**, *38*, 1477-1504. [Crossref], [Google Scholar], [Publisher]

[63] B. Gole, A.K. Bar, P.S. Mukherjee, *Chem. Commun.,* **2011**, *47*, 12137-12139. [Crossref], [Google Scholar], [Publisher]